Ab Initio Investigation of the Structure and Spectroscopy of Hydronium−Water Clusters

Andrzej L. Sobolewski*,† and Wolfgang Domcke‡

Institute of Physics, Polish Academy of Sciences, PL-02668 Warsaw, Poland, and Institute of Physical and Theoretical Chemistry, Technical University of Munich, D-85747 Garching, Germany

Received: October 16, 2001; In Final Form: January 14, 2002

Ab initio (MP2, CASSCF, CASPT2) and DFT/B3LYP calculations have been performed to explore the structures and the electronic and vibrational spectra of hydronium−water clusters as well as the corresponding cluster cations. Minimum-energy and transition-state structures have been optimized at the MP2 and DFT/B3LYP levels. Whereas protonated water clusters can exist both in Eigen-type structures, $H_3O^+(H_2O)_n$, as well as in Zundel-type structures, $H_5O_2^+(H_2O)_n$, the neutral radical clusters are found to prefer Eigen-type structures, $H_3O(H_2O)_n$. While $H_3O(H_2O)_3$, like the hydronium radical, is a metastable species, it exhibits a significantly higher barrier for hydrogen detachment (7 kcal/mol), indicating the possibility of kinetic stability of larger $H_3O(H_2O)_n$ clusters at low temperatures. Remarkably, hydronium−water clusters are charge-separated species, consisting of a hydronium cation and a localized electron cloud, which are connected by a water network. The vertical electronic excitation energies of the various $H_3O(H_2O)_n$ clusters are found to scatter between 1.1 and 3.0 eV, thus covering the energy range of the absorption spectrum of the hydrated electron. The vibrational spectra of $H_3O(H_2O)_n$ clusters exhibit the known fingerprint lines of H_3O^+ and of free OH groups interacting with an excess electron and thus provide direct evidence of their charge-separated character. The relevance of these findings for the radiation chemistry of water is briefly discussed.

1. Introduction

Size-selected water clusters, $(H_2O)_n$, have been extensively investigated both experimentally[1−7] and theoretically[8−17] in recent years. Water clusters serve as useful models for the understanding of the complex structural and dynamical properties of water in condensed phases. The structures of the energetically low-lying isomers of neutral water clusters are well-known from computational studies up to $n = 12$.[8−10,12,15]

Protonated water clusters, $H^+(H_2O)_n$, and negatively charged water clusters, $(H_2O)_n^-$, also are of prominent interest, serving as models of the solvation of cations and excess electrons, respectively, in water. Size-specific spectroscopy is easier for these charged species than for neutral clusters. Therefore, a considerable amount of spectroscopic data is available for $H^+(H_2O)_n$ and $(H_2O)_n^-$ clusters.[18−25]

One of the intriguing issues motivating the study of protonated water clusters is the elucidation of the anomalously high mobility of the proton in liquid water. The discussion of this issue began with Grotthuss' idea of "structural diffusion" nearly two centuries ago.[26] Two main structural models have emerged for the hydrated proton. Eigen[27] proposed the formation of a $H_9O_4^+$ complex in which a H_3O^+ core is strongly hydrogen-bonded to three H_2O molecules. Zundel,[28] on the other hand, suggested the idea of a $H_5O_2^+$ complex, in which the proton is shared between two H_2O molecules. Ab initio electronic-structure calculations on $H^+(H_2O)_n$ clusters up to $n = 8$,[29−34] vibrational spectroscopy,[19] and molecular dynamics simulations[35−38] have lead to the conclusion that the hydrated proton forms a fluxional defect in the hydrogen-bonded network, with both $H_9O_4^+$ and $H_5O_2^+$ occurring in the sense of "limiting" or "ideal" structures.

$(H_2O)_n^-$ clusters have been suggested to serve as microscopic analogues of the hydrated electron,[39] which is considered to be a classic example of a system in which a quantum mechanical particle (i.e., the excess electron) becomes localized through interaction with a medium.[40] Experimental investigations of the electron detachment energy spectra of $(H_2O)_n^-$ clusters[21,22] show the increase of the binding energy of the electron parallel to the cluster size. Ab initio investigations up to $n = 9$[41−45] indicate that linear "chainlike" species with an excess electron bound at the end by the dipole field are the most stable structures of these relatively small clusters.[24] The existence of anionic clusters representing the caging of the electron, such as a bowl-like $(H_2O)_6^-$ cluster, is discussed controversially in the current literature.[42,44]

Neutral radical clusters such as $H(H_2O)_n$ or $OH(H_2O)_n$ have found much less attention. On the experimental side, it is difficult to prepare these species and to obtain size-specific spectra. From the theoretical point of view, calculations are more involved for these open-shell species than for closed-shell systems such as $(H_2O)_n$ or $H^+(H_2O)_n$.

The hydronium radical, H_3O, may be considered as the smallest cluster of the type $H(H_2O)_n$. H_3O is a so-called Rydberg molecule, which is bound in Rydberg excited states but not in the ground electronic state. The barrier for decay into $H + H_2O$ is too low to allow for a significant lifetime.[46,47] H_3O and D_3O radicals have been formed by neutralization of ion beams, but only D_3O is sufficiently long-lived to be detected by mass spectroscopic techniques.[48] Hudgins and Porter have prepared $H_3O(H_2O)_n$ clusters by ion beam neutralization and have shown that the hydronium radical is stabilized by solvation.[49]

The H_3O radical has been the subject of a number of theoretical investigations,[46,47,50,51] mostly in the context of identifying radiative transitions between Rydberg states, stimulated by the observation of optical emission spectra of the

* To whom correspondence should be addressed. Fax: +48-22-8430926. E-mail: sobola@ifpan.edu.pl.
† Polish Academy of Sciences.
‡ Technical University of Munich.

10.1021/jp013835k CCC: $22.00
Published on Web 03/21/2002

ammonium radical by Herzberg.[52] An early paper by Schwartz[53] and more recent work by Muguet[54] have pointed out that the 3s → 3p absorption of H_3O falls into the energy range of the absorption spectrum of the hydrated electron. Muguet also has calculated the absorption spectrum of the dihydronium radical, H_5O_2.[55] Extensive calculations of global potential-energy surfaces of the H_3O system have been performed in the context of the $H + H_2O \rightarrow H_2 + OH$ reaction and the emission spectra of $OH-H_2$ exciplexes.[56−59] No calculations on $H(H_2O)_n$ clusters beyond H_5O_2 are known to the authors.

The relevance of water clusters containing the H radical for the rationalization of important chemical processes in liquid water has become apparent only relatively recently. Experimental[60−63] and theoretical[64−66] studies on the photochemistry of clusters of indole and phenol with water and ammonia independently have revealed that hydrogen transfer (rather than proton transfer) from the chromophore to the solvent is the dominant photochemical process in these systems. The calculations have shown that the hydrogen-transfer photochemistry is governed by an optically dark state of $^1\pi\sigma^*$ character, which is repulsive with respect to the NH stretching coordinate of indole and the OH stretching coordinate of phenol, respectively. Excited-state geometry optimization has revealed that the 1:1 cluster of indole (phenol) with water relaxes to a configuration in which an indolyl (phenoxyl) radical is hydrogen-bonded to a hydronium radical.[65,66] Calculations for indole (phenol)$(H_2O)_n$ clusters have shown, furthermore, that the preferred structure of the water network after hydrogen atom transfer is that of a solvated hydronium ion and a solvated diffuse electron cloud.[65,66]

It has been known for decades that UV excitation of indole and phenol in liquid water leads to the formation of solvated electrons with high quantum yields.[67,68] This and the computational findings of a photoinduced chromophore-to-cluster hydrogen-transfer process and of the spontaneous charge separation in $H_3O(H_2O)_n$ clusters[66] strongly suggest a close relationship between hydrated hydronium and the solvated electron, as conjectured earlier by Robinson and Muguet.[54,69] This conjecture is further supported by the computational finding[70] that a barrierless hydrogen-transfer reaction path exists in the first excited singlet state of the water dimer, leading to OH and H_3O radicals. It thus appears almost certain that the H_3O radical is involved in the sequence of ultrafast processes following photoabsorption in liquid water. A systematic investigation of $H_3O(H_2O)_n$ clusters is thus warranted for a better understanding of radiation-induced metastable defects in liquid water.

In the present work, we report the results of a comprehensive theoretical investigation of $H_3O(H_2O)_n$ clusters. The UMP2 and DFT methods were used for the optimization of the cluster geometries. At the stationary points, a vibrational normal-mode analysis was performed, and the resulting IR spectrum was calculated. The diffuse character of the 3s Rydberg electron indicates that it should be particularly susceptible to microsolvation. The effect of microsolvation on the stability of the clusters was investigated for H_3O and $H_3O(H_2O)_3$ by constructing the potential-energy (PE) profiles along the minimum-energy path for detachment of a hydrogen atom. In addition to the calculations of PE profiles, we have also analyzed the electronic wave function in terms of molecular orbitals and charge distribution. It has been found that with the increase of the cluster size the Rydberg electron detaches from the H_3O^+ core and (micro)solvates in the network of water molecules. The calculated electron excitation energies of the microsolvated H_3O radical are in support of the idea that the hydronium radical may be a precursor of the hydrated electron produced by UV irradiation of liquid water.

We also have calculated the equilibrium geometries and vibrational spectra of several small protonated water clusters with the same theoretical methods. The ground-state structures of the protonated water clusters up to $n = 8$ have been optimized at different levels of theory by several authors[29−34] and need not be discussed in detail here. The results on $H^+(H_2O)_n$ clusters are included here to establish comparisons with previous work and to aid in the interpretation of the structures and vibrational spectra of hydronium−water clusters.

2. Computational Methods

The ground-state geometry of the $H^+(H_2O)_n$ and $H(H_2O)_n$ clusters (henceforth referred to as H^+W_n and HW_n clusters, respectively) was optimized with the restricted and unrestricted Hartree−Fock second-order Møller−Plesset (MP2 and UMP2, respectively) methods. Because for larger clusters these methods become quite expensive, the geometries were also optimized at the density-functional-theory (DFT) level with the B3LYP functional. The comparison between the ab initio and DFT results obtained for smaller clusters ($n \leq 5$) leads to the conclusion that both methods give comparable results. Thus, only the DFT method was used for geometry optimizations and vibrational frequency calculations of larger clusters.

The standard 6-31+G** split-valence double-ζ Gaussian basis set augmented with polarization functions on all atoms and with diffuse functions on the oxygens was supplemented with an additional set of diffuse s and p Gaussian functions of exponent $\eta = 0.02$, located on the oxygens to provide additional flexibility for the description of the Rydberg electron. This basis set was used in the geometry optimizations and in the calculation of vibrational absorption spectra of all clusters studied. The calculations of geometries and vibrational spectra have been performed with the Gaussian 98 package.[71]

The vertical excitation energies of the lowest doublet excited states of hydronium−water clusters have been obtained with the CASPT2 method (second-order perturbation theory based on the CASSCF reference).[72] The active space for the CASPT2 calculations includes the HOMO 3s orbital of the H_3OW_n cluster and the three lowest unoccupied orbitals of 3p Rydberg character. The CASPT2 calculations were performed with the MOLCAS-4 package[73] using the ANO-L basis set of split-valence double-ζ quality with polarization functions on all atoms and with additional diffuse s and p Gaussian functions of exponent $\eta = 0.02$ located on the oxygens.

The CASPT2 calculations performed for H_3OW_n clusters with a larger active space correlating several electrons show that the 3s Rydberg electron is essentially decoupled from the other electrons and that the wave function of the ground state of the radical clusters is dominated by a single reference. The single-reference CASSCF calculation is equivalent to a restricted open-shell Hartree−Fock (ROHF) calculation. Therefore, the ROHF method has been used for the determination of the minimum-energy path for detachment of the hydrogen atom from the cluster. For the construction of the reaction path for hydrogen detachment, the coordinate-driven minimum-energy-path approach was adopted, that is, for a given value of the OH bond length all remaining nuclear coordinates were optimized. To incorporate dynamic electron-correlation effects, single-point calculations at optimized geometries were performed with the CASPT2 method.

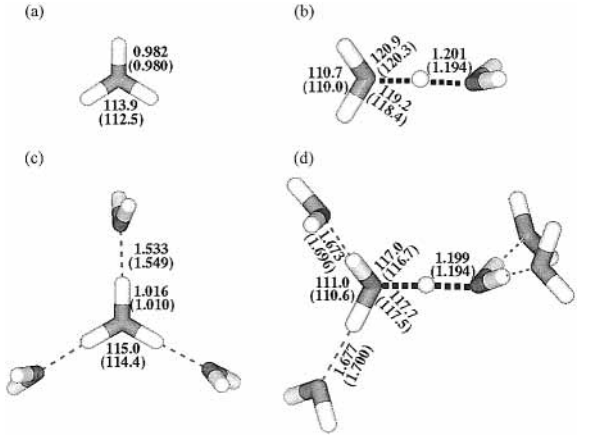

Figure 1. DFT/B3LYP equilibrium geometry in the electronic ground state of H_3O^+ (a) and $H_5O_2^+$ (b). The numbers in parentheses denote the MP2-optimized values of bond lengths (in Å) and bond angles (in deg). The equilibrium geometries of $H_3O^+W_3$ and $H_5O_2^+W_4$ are displayed in panels c and d, respectively.

3. Results and Discussion

3.1. Protonated Water Clusters. *A. Structures.* The equilibrium structures of the H^+W_n clusters for $n = 1$, 2, 4, and 6, optimized with DFT and MP2 methods, are shown in Figure 1. They represent the "bare" Eigen-type unit, H_3O^+, (Figure 1a) and Zundel-type unit, $H_5O_2^+$, (Figure 1b). The corresponding clusters with a first solvation shell, $H_3O^+W_3$ and $H_5O_2^+W_4$, are shown in Figure 1, parts c and d, respectively. As is well-known, the hydronium cation has C_{3v} symmetry. It is only slightly pyramidal: the sum of the three bond angles is 341.7° (337.5°) for the DFT (MP2) optimized structures. The structure is in good agreement with that reported in other works.[31] The $H_5O_2^+$ dihydronium cation has an equilibrium geometry of C_2 symmetry, with the excess proton lying midway between the two water molecules. The two H_3O subunits are slightly less pyramidal than the hydronium cation itself. The sum of the bond angles around oxygen is 350.8° (348.7°) at the DFT (MP2) levels. The two water molecules are rotated with respect to each other around the C_2 symmetry axis by a dihedral angle of 96.7° (DFT) and 97.1° (MP2). All of these results are in good agreement with other works of a similar level of sophistication.[29−33]

It should be stressed that all vibrational frequencies of the structures in Figure 1 are real, that is, the structures represent true local minima of the PE surface. The controversy in the literature concerning the symmetric structure of the Zundel unit (C_2 symmetry, with the proton in midway of the two oxygens) or asymmetric structure (C_1 symmetry, with the proton more tightly bound to one oxygen)[19,31] is mainly related to deficiencies in the treatment of dynamical electron correlation effects. Both at the DFT/B3LYP and at the MP2 levels of theory the C_2 structures of $H_5O_2^+$ and $H_5O_2^+W_4$ represent true minima of the PE surfaces of these systems. There is no such controversy concerning the Eigen-type unit, $H_3O^+W_n$, $n = 0$, 3. The existing theoretical data suggest that the structure of C_{3v} symmetry represents a true minimum of the ground-state PE surface (see refs 19 and 31 and references therein). There is, however, a very small barrier for inversion, the transition-state structure of D_{3h} symmetry being only by fraction of a kcal/mol higher in energy.[19]

Complexation of both units, H_3O^+ and $H_5O_2^+$, with a first solvation shell of water only marginally disturbs their geometries. The OH bond lengths of the central units pointing in the direction of the water molecules of the first solvation shell are slightly lengthened compared to the bare units, and strong hydrogen bonds are formed. Solvation slightly changes the pyramidization of the H_3O units. While the Eigen-type unit gets more planar, the Zundel-type unit pyramidizes slightly more upon solvation.

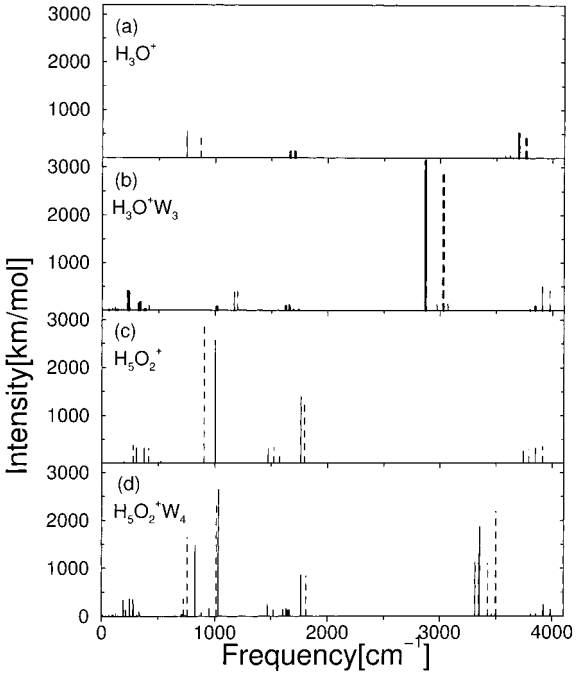

Figure 2. Vibrational spectra of H_3O^+ (a), $H_3O^+W_3$ (b), $H_5O_2^+$ (c), and $H_5O_2^+W_4$ (d), calculated in the harmonic approximation at the DFT/B3LYP (solid sticks) and the MP2 (dashed sticks) levels. Bold sticks denote transitions to degenerate (E) vibrational levels; thin sticks represent transitions to nondegenerate (A) levels for the systems with 3-fold symmetry.

It is perhaps worth noting that the $H_3O^+W_3$ structure of Figure 1c has approximate D_{3h} symmetry, the terminal water molecules being almost perpendicular to the corresponding vertical symmetry plane. This structure is very different from that of the neutral counterpart, as will be seen in section 3.2.

B. Vibrational Spectra. The harmonic vibrational spectra of the structures displayed in Figure 1 are shown in Figure 2. The spectra obtained from DFT/B3LYP and MP2 calculations are presented for comparison of the methods. Figure 2 reveals satisfactory agreement of the spectra calculated with the two theoretical methods. The main differences between the DFT and MP2 spectra arise from differences of the vibrational frequencies which, particularly those involving OH stretching, are predicted higher with the MP2 method than with the DFT method.

For H_3O^+, Figure 2a, we obtain a symmetric OH stretch frequency of 3577 cm^{-1} (3621 cm^{-1}) and intensity of 34 km/mol (40 km/mol) with the DFT (MP2) method. The respective numbers for the degenerate asymmetric OH stretch obtained with the two methods are 3698 cm^{-1} (3764 cm^{-1}) and 516 km/mol (513 km/mol). These numbers are in excellent agreement with those obtained in ref 31 at the DFT level employing the Perdew functional. Inspecting results of ref 31, one can notice, however, an apparent misassignment of the spectra. The two degenerate e-type vibrations must have the same frequencies and intensities by definition. In ref 31, one of the components of the asymmetric OH stretch has been misassigned as the symmetric vibration and vice versa. The same misassignment has been made for the $H_9O_4^+$ cluster.

Attachment of the first solvation shell to the H_3O^+ unit (the $H_3O^+W_3$ cluster) reduces significantly the OH stretching

frequencies due to hydrogen bonding (Figure 2b), as expected. The DFT frequency (intensity) is now 2868 cm^{-1} (3146 km/mol) for the degenerate asymmetric vibration and 2970 cm^{-1} (124 km/mol) for the symmetric OH stretch vibration. An important feature of the IR spectrum of the $H_3O^+W_3$ cluster compared to the H_3O^+ cluster is a remarkable increase of intensity of the OH stretching vibrations. The intensity of the degenerate asymmetric stretch vibration, in particular, increases by a factor of 6 upon solvation and completely dominates the spectrum. Note that each component of this vibration has an intensity of about 3000 km/mol, so the intensity of the band is twice as large. This result indicates that the asymmetric stretching vibration of the $H_3O^+W_3$ cluster modulates strongly the charge-density distribution, an effect which is apparently less pronounced in the bare hydronium cation. The effect is predicted independently of the theoretical approach (DFT or MP2). In this respect, our results are in good agreement with those of ref 31.

The IR absorption spectra of the bare Zundel-type unit, $H_5O_2^+$ and the solvated Zundel unit, $H_5O_2^+W_4$, are presented in Figure 2, parts c and d, respectively. The spectra are qualitatively different from those of the Eigen-type complexes discussed above. The main difference is the absence of strong bands near 3000 cm^{-1}, characteristic for the OH stretching vibrations of the Eigen-type cluster $H_3O^+W_3$. Indeed, the strongest lines are calculated in the region of 1000−2000 cm^{-1}, the frequency range typical for HOH bending vibrations. The two strongest lines of the IR spectrum of the $H_5O_2^+$ cluster (Figure 2c) at 1004 cm^{-1} (2596 km/mol) and at 1763 cm^{-1} (1395 km/mol) are identified as mostly involving the proton-transfer (PT) coordinate between the two oxygen atoms, the PT coordinate being strongly coupled to the HOH bending (scissoring) vibration of the neighboring waters. The respective frequencies and intensities of these bands calculated at the MP2 level are 905 cm^{-1} (2906 km/mol) and 1795 cm^{-1} (1250 km/mol). This again confirms the consistency of the results calculated by these two methods.

Complexation of $H_5O_2^+$ with the first solvation shell (Figure 2d) influences the IR lines associated with the PT mode only marginally, in contrast to the Eigen unit, yielding 1033 cm^{-1} (2643 km/mol) and 1766 cm^{-1} (863 km/mol), respectively. An additional intense low-frequency line at 827 cm^{-1} (1478 km/mol) also involves the PT-type motion coupled to the out-of-plane bending of the neighboring waters. The group of four intense bands around 3300 cm^{-1} (only three of them are resolved on the scale of Figure 2d) with frequencies of 3317, 3351, 3353, and 3356 cm^{-1} and intensities of 1132, 1293, 587, and 1865 km/mol, respectively, involve the OH stretching motion of the two water molecules of the $H_5O_2^+$ central unit.

Overall, the results for protonated water clusters reveal that the two theoretical methods, DFT/B3LYP and MP2, are mutually consistent. Despite small quantitative differences in optimized geometries and in IR absorption spectra calculated by the two methods, the picture of the behavior of an excess proton in small water clusters is independent of the applied method. The present results are also in agreement with those of ref 31 obtained with a different exchange-correlation functional. We want, in particular, to refer to the work of Ciobanu et al.[34] in which several isomers of the H^+W_8 cluster were optimized and IR absorption spectra were calculated with the use of similar theoretical methods. They have found that the intense IR-active modes in the 690−1000 cm^{-1} range are the "true" PT modes, which essentially involve the displacement of the excess proton between two oxygen atoms, while those above 2800 cm^{-1} involve very little central proton motion. The latter arise primarily from the stretching of the outer OH bonds of the $H_5O_2^+$ unit. Ciobanu et al. have concluded that the position of the excess proton in the water cluster is mainly determined by the geometry of the solvating shells of water. The transition from the symmetric $H_5O_2^+$-like to the non-symmetric H_3O^+-like configuration is accompanied by a systematic decrease of the spectral intensity below 2800 cm^{-1}. Our results are fully consistent with this conclusion.

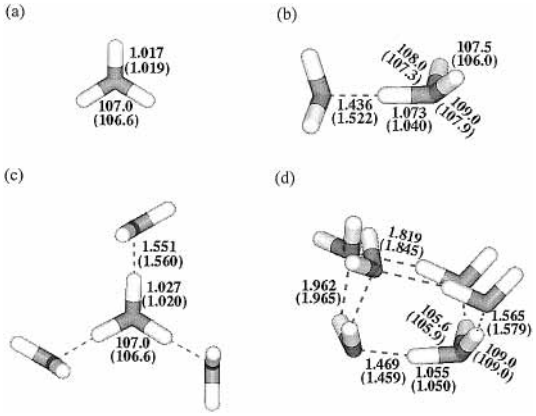

Figure 3. DFT/B3LYP equilibrium geometry in the electronic ground state of the H_3OW_n clusters: (a) $n = 0$; (b) $n = 1$; (c) $n = 3$; (d) $n = 5$. The numbers in parentheses denote the MP2-optimized values of bond lengths (in Å) and bond angles (in deg).

3.2. Hydronium−Water Clusters. *A. Geometric and Electronic Structures.* In Figure 3, we present the optimized structures of selected H_3OW_n clusters, the neutral counterparts of the $H_3O^+W_n$ cations discussed in the preceding section. Comparing the relevant H_3OW_n structures in Figure 3 to the corresponding cations (Figure 1), one can notice a considerable difference in their geometries. Already for the bare H_3O^+ cation, the neutralization influences significantly the geometry. The hydronium radical has C_{3v} symmetry like its cation, but the OH bond lengths increase by about 0.05 Å (0.04 Å) at the DFT (MP2) level, and the system becomes more pyramidal: the sum of the three bond angles decreases by 15.60° (17.70°). Neutralization of the $H_5O_2^+$ cation results in the relaxation of the Zundel-type structure of C_2 symmetry (Figure 1b) to the asymmetric H_3O-H_2O structure of Figure 3b, in which the excess hydrogen is more tightly bound to one water molecule and forms a fairly strong hydrogen bond to the other. The C_2 structure of the H_5O_2 cluster is, however, higher by only 0.4 kcal/mol (1.1 kcal/mol) than the C_1 structure at the DFT (MP2) level, thus indicating a very flat PE function for vibrational motion of the hydrogen atom between the two water molecules.

Solvation of the H_3O and H_5O_2 clusters with the first shell of water results in even more pronounced changes of geometry with respect to the cationic counterparts. The almost planar (approximate D_{3h} symmetry) $H_3O^+W_3$ cation (Figure 1c) relaxes upon neutralization to the strongly pyramidal (C_3 symmetry) structure of Figure 3c. The length of the hydrogen bond between H_3O and H_2O is 1.551 Å (1.560 Å) at the DFT (MP2) level, indicating a fairly strong H-bond, nearly as strong as that in the cation (1.533 Å (1.549 Å)). It is worth noting that the C_{3v} isomer of the H_3OW_3 cluster, shown in Figure 4a, is only 0.6 (1.0) kcal/mol higher in energy than the C_3 structure of Figure 3c. Both the C_3 and C_{3v} structures represent stable minima on the PE surface of the H_3OW_3 cluster, as confirmed by the normal-mode analysis.

The C_2 Zundel-type ion solvated with the first shell of water ($H_5O_2^+W_4$ of Figure 1d) relaxes to the C_s structure of Figure

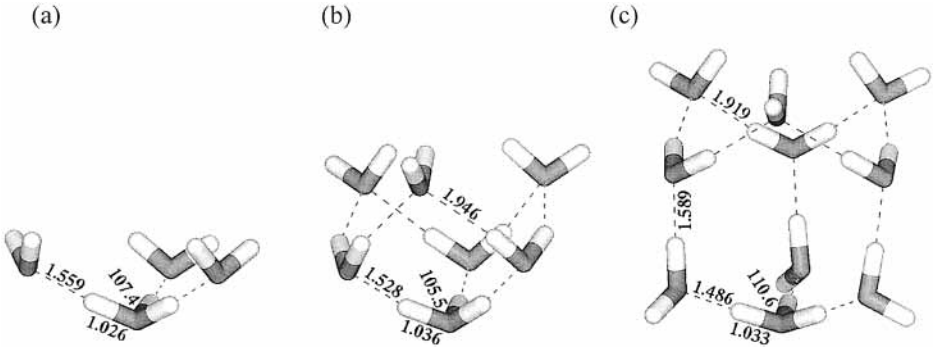

Figure 4. DFT/B3LYP equilibrium geometry in the electronic ground state of the H_3OW_{3m} clusters: (a) $m = 1$ (C_{3v} isomer), (b) $m = 2$, (c) $m = 3$. The numbers denote DFT/B3LYP-optimized geometry parameters (bond lengths in Å, bond angles in deg).

3d upon neutralization. Comparison of the H_3OW_5 structure (Figure 3d) with the H_3OW_3 structure (Figure 3c) shows an astonishing similarity of the geometry parameters of the three water molecules directly H-bonded to the H_3O unit. In both systems, these H-bonds are fairly strong as indicated by their relatively short lengths. On the other hand, the two terminal water molecules of the H_3OW_5 cluster are remarkably more weakly H-bonded. This indicates that they should be considered as belonging to the second solvation shell of the H_3O unit. These findings indicate that $H(H_2O)_n$ neutral radical clusters have a strong propensity to form 3-fold coordinated H-bond structures around the H_3O radical.

Indeed, if the H_3OW_5 cluster is augmented with one additional water molecule, the 3-fold symmetry axis of the H_3O unit is restored and the minimum-energy structure of the H_3OW_6 cluster has C_{3v} symmetry (Figure 4b). One can see that the second solvation shell is more weakly bound than the first one (H-bond lengths of 1.946 Å and 1.528 Å, respectively, at the DFT/B3LYP level). Also, this cluster possesses two stable minima of C_{3v} and C_3 symmetry, the former being by about 3.7 kcal/mol more stable than the latter at this level of theory. In the C_3 structure, the H_3O unit binds somewhat more strongly the shells of water (H-bond lengths of 1.657 Å and 1.501 Å, respectively).

The tendency of conserving the 3-fold axis of symmetry is also observed in larger clusters of the type H_3OW_{3m}. In Figure 4c, we present the DFT-optimized structure of the H_3OW_9 cluster. It has overall C_3 symmetry, but one can notice that the two terminal shells of water have approximate C_{3v} symmetry, very similar to the geometry of the water shells in the H_3OW_6 cluster (Figure 4b), while the first solvation shell has a geometry that is similar to that of the H_3OW_3 cluster (Figure 3c).

A clue for explanation of the remarkable difference between the structures of the hydrated hydronium clusters and their corresponding cations is provided by an analysis of the electronic structure of the neutral clusters, as illustrated in Figure 5. This figure displays the singly occupied ROHF molecular orbital of the H_3OW_n clusters. It is seen that the 3s Rydberg-type orbital of H_3O (Figure 5a) and H_5O_2 (Figure 5b) detaches from the H_3O^+ ionic core in the H_3OW_n, $n > 1$, systems. In the H_3OW_3 complex (Figure 5c), the hydronium radical cation forms strong H-bonds with three water molecules, which in turn solvate the charge distribution of the unpaired electron. The process of charge separation progresses with the addition of further water molecules (Figure 5d−f). In the H_3OW_6 (Figure 5e) and H_3OW_9 (Figure 5f) complexes, two and three water shells separate the H_3O^+ cation and the electronic cloud, respectively.

The very stable and rigid H_3O^+ ion apparently enforces a 3-fold symmetry of the clusters of the type H_3OW_{3m}, $m = 1, 2, 3$, and the unpaired electron prefers to localize outside the H-bonded water network. The hydronium radical thus dissolves into a solvated hydronium cation and a solvated electron cloud in an aqueous environment by a spontaneous charge-separation process.

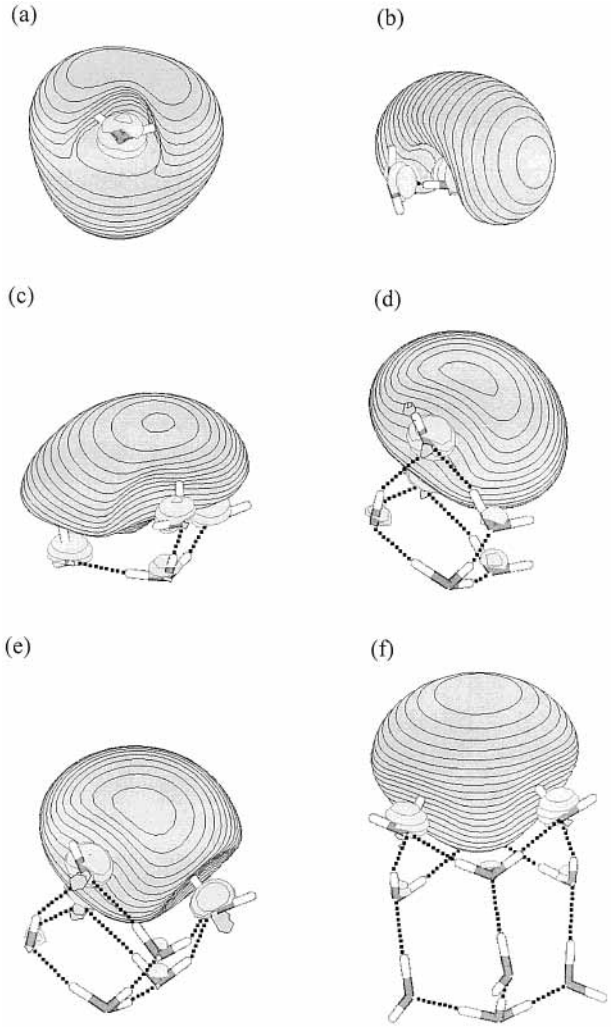

Figure 5. The singly occupied highest ROHF molecular orbital of the H_3OW_n clusters: (a) $n = 0$; (b) $n = 1$; (c) $n = 3$; (d) $n = 5$; (e) $n = 6$; (f) $n = 9$.

The increasing charge separation in the H_3OW_n clusters is reflected by the increase of the dipole moment with the increase of the cluster size as shown in Figure 6. For the clusters with "closed" water shells, H_3OW_{3m}, $m = 1, 2, 3$, the increase of the dipole is an almost linear function of the number of water molecules attached to the H_3O unit. All of these clusters have 3-fold symmetry, and the dipole moment is directed along the symmetry axis. The dipole moments of the less symmetric

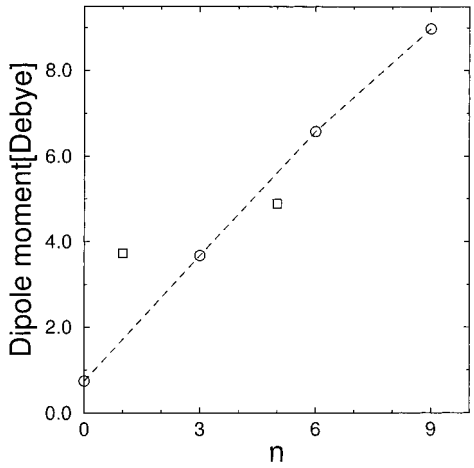

Figure 6. CASSCF dipole moments of H_3OW_n clusters, as a function of the number of water molecules attached to the H_3O unit. The $n = 0$, 3, 6, and 9 clusters are shown as circles, $n = 1$, 5 as squares.

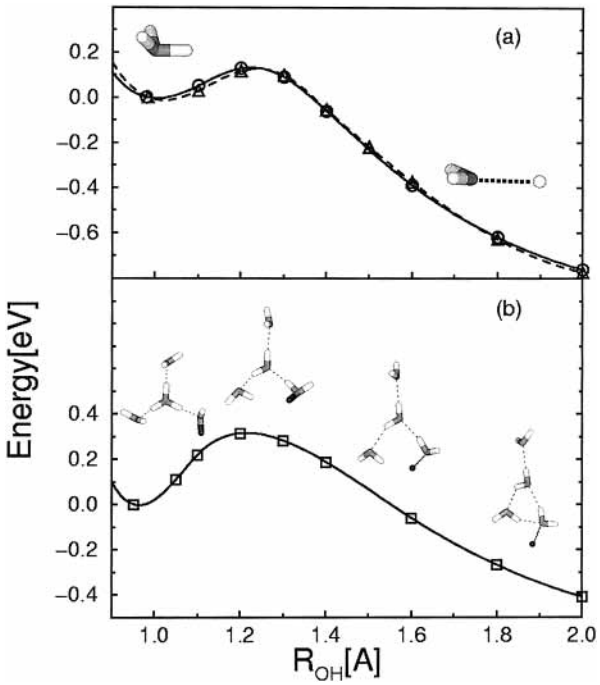

Figure 7. MP2 PE functions of the electronic ground state of H_3O (a) and H_3OW_3 (b), calculated along the ROHF-optimized minimum-energy reaction path for hydrogen detachment. Triangles connected by the dashed line in panel a represent MP2 energies calculated along the MP2-optimized reaction path.

clusters, $H_3OW_1(C_1)$ and $H_3OW_5(C_s)$, scatter with respect to the H_3OW_{3m} family. It is particularly worth noting the significant polarity of the H_5O_2 cluster in comparison with the hydronium radical.

Finally, we want to stress that the lowest-energy 3-fold symmetric stiff "nanotubes" of the H_3OW_{3m} clusters (Figures 4 and 5), with H_3O^+ on one end and the electron at the other end, are highly ordered and therefore of low entropy. At finite temperature, a balance between energy and entropy matters, which can limit the growth of the nanotubes at the expense of less-symmetric and energetically higher isomers. We cannot answer the question of the distribution of the H_3OW_n clusters in liquid water by zero-temperature calculations. It has to remain open at the moment.

B. Stability of the Hydrated Hydronium Radical. Figure 7 shows MP2 PE profiles calculated along the minimum-energy path for the detachment of a hydrogen atom from H_3O (a) and H_3OW_3 (b). Figure 7a illustrates the well-known fact that the hydronium radical is less stable by about 21 kcal/mol than the $H + H_2O$ dissociation limit.[46,47] The local PE minimum of C_{3v} symmetry is separated by a barrier of about 3.6 kcal/mol from the $H + H_2O$ dissociation channel.[46,47] The present result of 2.7 kcal/mol is in reasonable agreement with this value. Another result illustrated by in Figure 7a is the remarkable similarity of the PE functions for hydrogen detachment determined by two different theoretical approaches, MP2 single-point calculations along the MP2-determined minimum-energy path (dashed line with triangles) and along the ROHF-determined minimum-energy path (full line with circles). This result justifies the use of the cheaper ROHF geometry optimization to study the stability of larger clusters.

Figure 7b shows the corresponding energy profile for the removal of a hydrogen atom from the H_3OW_3 cluster. The rearrangement of the cluster during this dissociation process is illustrated by several snapshots of the geometric structure along the reaction path. The hydrogen-detachment process involves a hydrogen shift from the central hydronium unit to one of the terminal waters via a Zundel-type transition state. The terminal hydronium then dissociates, yielding a W_4 cluster and an H atom.

Upon detachment of the proton, the 3s Rydberg-type singly occupied highest ROHF molecular orbital of H_3O and H_3OW_3 clusters (Figure 5, parts a and c, respectively) contracts and evolves to the 1s orbital of hydrogen. The transformation occurs near the top of the barrier for the reaction.

It is seen that hydrogen detachment from H_3OW_3 is a considerably less exothermic process than hydrogen detachment from H_3O. Moreover, the barrier separating H_3OW_3 from the dissociation channel is found to be 7.0 kcal/mol and is thus significantly larger than the barrier in H_3O. This finding is in agreement with the results of neutralized ion beam experiments, which have demonstrated enhanced stability of the H_3OW_3 cluster.[49]

Calculations of the type shown in Figure 7b have to be extended to larger clusters. It is strongly suggested by the present preliminary results, however, that H_3OW_{3m}, $m = 1, 2, 3$, clusters are considerably more stable and long-lived than the bare hydronium radical. It is an interesting open question whether H_3OW_n clusters are thermodynamically stable with respect to hydrogen detachment for $n \rightarrow \infty$. In any case, larger H_3OW_n clusters should be at least kinetically stable with respect to the hydrogen-detachment reaction at low temperatures.

It has recently been shown by Jouvet and collaborators[61,62] and Fujii and collaborators[63] that long-lived $NH_4(NH_3)_n$ clusters are formed by UV excitation of phenol−ammonia clusters via a hydrogen-transfer reaction in the excited state and subsequent dissociation. Ishiuchi et al. have shown that it is possible to obtain size-specific IR spectra of these clusters by double-resonance techniques.[63] Although excited-state hydrogen transfer is less facile in phenol−water than in phenol−ammonia clusters,[61,62,66] it should be possible to obtain in this way spectroscopic information on size-selected H_3OW_n clusters.

C. Electronic and Vibrational Spectra of H_3O and Hydrated H_3O. It has been noted previously that the 3s → 3p transition in H_3O is expected to fall into the energy range of the absorption spectrum of the hydrated electron.[53,69] More recently, Muguet has calculated the vertical excitation spectrum of hydronium (and dihydronium) with a MCSCF-propagator method.[54,55] He reported 2.0 eV for the 3s → 3p excitation energy of bare H_3O. Employing a reaction field continuum model of solvation,

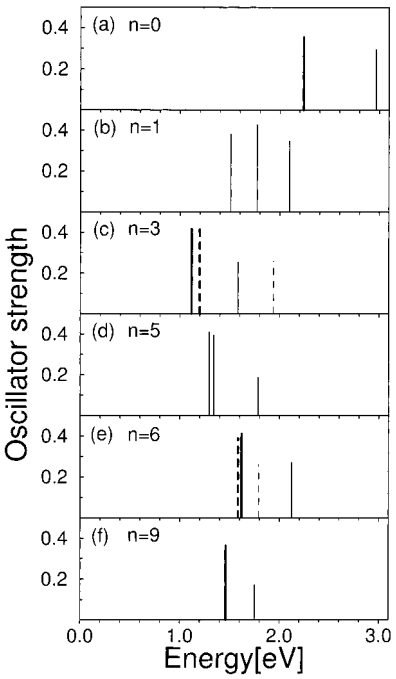

Figure 8. Vertical electronic excitation energies and oscillator strengths of H_3OW_n, $n = 0$, 1, 3, 5, 6, 9, clusters, calculated at the CASPT2 level. Bold sticks denote transitions from the ground state to the degenerate $^2E(p_{x,y})$ state; thin sticks represents transitions to the $^2A(p_z)$ state for the clusters with 3-fold symmetry. Dashed sticks in panels c and e represent the spectra of the isomers of C_{3v} and C_3 symmetry, respectively.

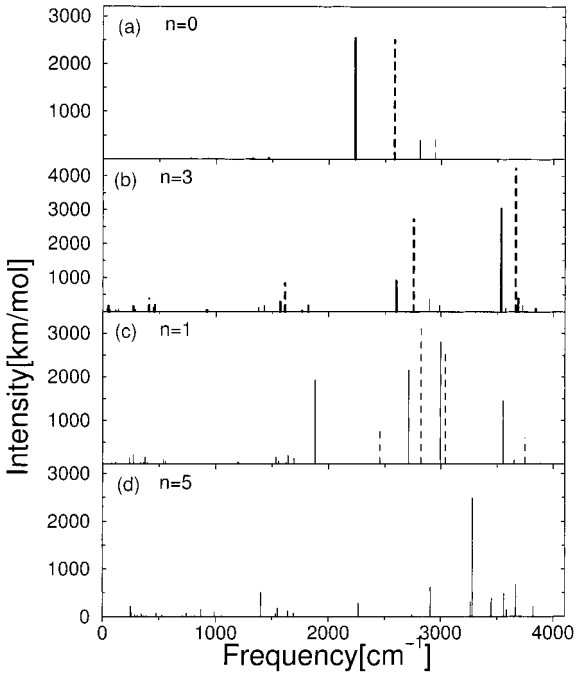

Figure 9. Vibrational spectra of H_3OW_n clusters, calculated in the harmonic approximation at the DFT/B3LYP (solid sticks) and the MP2 (dashed sticks) levels: (a) $n = 0$; (b) $n = 3$; (c) $n = 1$; (d) $n = 5$. Bold sticks denote transitions to degenerate (E) vibrational levels; thin sticks represent transitions to nondegenerate (A) levels for the systems with 3-fold symmetry.

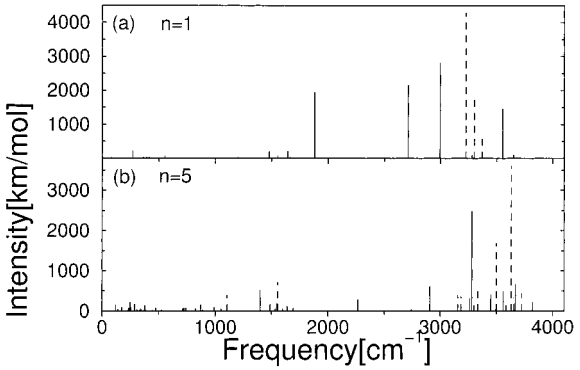

Figure 10. Vibrational spectra of the H_3OW_1 (a) and H_3OW_5 (b) clusters, calculated in the harmonic approximation at the DFT/B3LYP level. Solid sticks denote the spectra calculated at the stable (C_1 and C_s, respectively) minima of the clusters, while the dashed sticks denote spectra calculated at the C_2 transition-state structures.

Muguet has estimated the excitation energy of hydronium in liquid water to be in the range 1.8−2.0 eV.[54]

Figure 8 shows the present CASPT2 vertical electronic excitation energies and oscillator strengths of H_3OW_n clusters for $n = 0$, 1, 3, 5, 6, and 9. The thick bar represents the excitation energy and oscillator strength of the degenerate $^2E(p_{xy})$ state (to be multiplied by two), while the thin bar represents the $^2A(p_z)$ state, for the complexes with 3-fold symmetry. The dashed lines in panels c and e represent the spectra of the higher-energy isomers of C_{3v} and C_3 symmetry, respectively (cf. section 3.2A).

The excitation energy of the ^2E state of H_3O is found to be 2.20 eV (Figure 8a), in good agreement with the result of Muguet.[54] It is seen that microsolvation of H_3O by a single water molecule shifts the excitation energy markedly to the red (Figure 8b). This reflects the fact that H_3OW_n is not a solvated Rydberg molecule (for which a blue shift of the absorption spectrum is expected), but a microsolvated electron−ion complex. Completion of the first solvation shell in H_3OW_3 results in a further red shift of the absorption spectrum (Figure 8c). Because the H_3OW_3 cluster has two stable isomers of C_3 and C_{3v} symmetry that differ only marginally in energy (1 kcal/mol), we have included the absorption spectra of both isomers in Figure 8c. One can notice a remarkable sensitivity of the absorption spectrum to even small changes of the cluster geometry. The lowering of the 3-fold symmetry of the H_3OW_3 cluster to C_s in the H_3OW_5 cluster splits the degeneracy of the ^2E state and shifts the bands slightly to the blue (Figure 8d). Completion of the second solvation shell in the H_3OW_6 cluster (Figure 8e) shifts the excitation energies further to the blue. Addition of the third solvation shell of water in the H_3OW_9 cluster (Figure 8f), results in a slight red shift of the spectrum and a decrease of the $^2E-{}^2A$ splitting. The sum of the oscillator strengths in all systems is close to unity, decreasing slightly for larger clusters.

In view of the sensitivity of the vertical excitation energies to cluster size and cluster geometry, we shall not discuss the electronic spectra of Figure 8 in detail. It suffices to stress that the calculated excitation energies essentially cover the energy range of the absorption of the hydrated electron, which extends from about 0.8 to about 3.0 eV.[39] Figure 8 suggests that the electronic absorption spectrum of a statistical distribution of H_3OW_n clusters can provide a partial explanation of the large width of the absorption spectrum of the hydrated electron. The inclusion of nuclear-motion effects is indispensable, of course, for a quantitative simulation of the spectrum.

The calculated vibrational spectra of the H_3OW_n clusters are shown in Figures 9−11. The spectra have been obtained in the harmonic approximation with the DFT/B3LYP method. For smaller clusters (H_3O, H_3OW_1, and H_3OW_3), the DFT/B3LYP spectra have been compared with the spectra obtained at the MP2 level (dashed lines in Figure 9a−c). The good qualitative

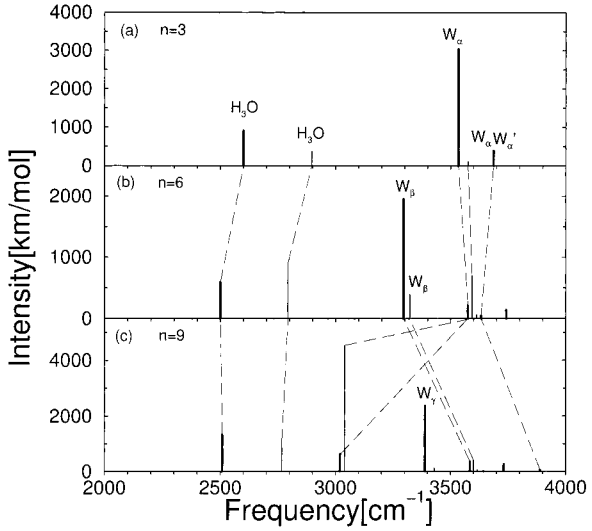

Figure 11. Vibrational spectra of H_3OW_3 (a), H_3OW_6 (b), and H_3OW_9 (c) clusters, calculated in the harmonic approximation at the DFT/B3LYP level. Bold sticks denote transitions to degenerate (E) vibrational levels; thin sticks represent transitions to nondegenerate (A) levels. The dashed lines connect the OH stretching bands of the central H_3O^+ unit of the clusters and of the successive shells of water (W_α, W_β, W_γ).

agreement supports the reliability of the DFT/B3LYP results for the larger clusters. Thick bars represent degenerate vibrational levels for the complexes with 3-fold symmetry (their intensity has to be multiplied by two); thin bars represent nondegenerate levels.

Although the harmonic approximation is questionable for H_3O (cf. Figure 7a), the H_3O spectrum has been included in Figure 9a to point out that already the bare H_3O radical exhibits a very intense absorption of the OH stretch vibration. Its intensity exceeds that of the most intense absorption of the H_2O molecule by nearly 2 orders of magnitude and also exceeds that of the H_3O cation (see Figure 3a). For H_3OW_3 (Figure 9b), an even more intense absorption, $I \approx 6000$ km/mol (8000 km/mol) at the DFT (MP2) level, is predicted near 3500 cm^{-1}. Similar intense absorption lines around (and above) 3000 cm^{-1} are obtained also for the H_3OW_1 (Figure 9c) and for the H_3OW_5 (Figure 9d) complexes.

The IR absorption spectra of the H_3OW_n clusters are remarkably different from the spectra of their ionic counterparts shown in Figure 2. This can partially be explained by the differences in the geometric structure of the neutral and ionic species. This applies, in particular, to the bare Zundel-type unit (Figures 2c and 9c) as well as to the Zundel unit solvated with the first shell of water molecules (Figures 2d and 9d). These ionic clusters have C_2 equilibrium geometry, with the proton midway between the two oxygen atoms (Figure 1b,d), whereas their neutral counterparts (Figure 3b,d) have lower symmetry, the hydrogen atom being valence-bonded to the water molecule. As a result, the absorption bands involving the OH stretching motion of the shared proton in the ionic clusters are lower in energy (1000−2000 cm^{-1}) than those of the corresponding neutral clusters (2000−3000 cm^{-1}). The C_2 transition-state structure of the H_3OW_1 cluster is only marginally less stable than the C_1 minimum. This calls the applicability of the harmonic approximation into question in this case. In the H_3OW_5 complex, the energy of the C_2 transition-state structure lies 6.8 kcal/mol (DFT/B3LYP level) above the C_s minimum structure, because the rearrangement of the equilibrium structure involves breaking of some of the hydrogen bonds. This energy is still comparable to the harmonic frequency of the OH stretching vibrations.

To illustrate this point, we compare in Figure 10 the IR absorption spectra of the H_3OW_1 and H_3OW_5 complexes obtained at their equilibrium and transition-state geometries, respectively. Solid sticks denote the spectra of the equilibrium structures; dashed sticks represent the spectra of the transition-state structures. In both clusters, the C_2 Zundel-type structure represents a first-order saddle point between the equilibrium structures of C_1 and C_s symmetry. The single imaginary frequency of 752 cm^{-1} (H_3OW_1) and 139 cm^{-1} (H_3OW_5) mostly involves the displacement of the shared hydrogen atom between two oxygen atoms. Figure 10 illustrates the significant sensitivity of the harmonic vibrational spectra, particularly in the range of the OH stretching vibrations, to the location of the excess hydrogen atom, indicating strong anharmonic coupling of the hydrogen-transfer coordinate with the OH stretch coordinates in these clusters. The vibrational motion of the excess hydrogen atom thus cannot properly be described within harmonic approximation. The strong anharmonic coupling of the OH stretch modes with the hydrogen-transfer mode is expected to result in a significant broadening of the OH stretch vibrational bands. In particular, the imaginary frequency of 752 cm^{-1} (H_3OW_1) polarizes strongly electron density of the cluster as indicated by its intensity (about 4000 km/mol).

The clusters of the type H_3OW_{3m}, $m = 1, 2, 3$, with closed solvation shells around the H_3O radical are more rigid with respect to the motion of the excess hydrogen atom. They are also expected to be more stable with respect to the dissociation of the hydrogen atom as discussed above. In this case, the harmonic approximation should be reasonably accurate. Because these clusters seem to represent the best candidates for experimental investigations, we present a more detailed analysis of the most prominent bands in their IR absorption spectra in Figure 11.

The most intense OH stretching absorption bands above 3000 cm^{-1} in the H_3OW_{3m}, $m = 1, 2, 3$, clusters are associated with the water molecules in the terminal solvation shell of the H_3O unit, that is, within the first solvation shell of the electron cloud. The OH stretch vibration of the H_3O^+ core is less intense and located near 2500 cm^{-1}. In the H_3OW_9 cluster, the very strong line around 3000 cm^{-1} is assigned to the OH stretch vibration of the first solvation shell of the H_3O unit. An analysis of the character of the normal mode shows that this vibration is strongly coupled with the OH stretch of the H_3O^+ core. This may indicate that the ionic character of the H_3O^+ core extends to the first solvation shell for larger clusters.

Intense IR absorption bands in the range of 3200−3400 cm^{-1} have been detected by Johnson and collaborators in negatively charged water clusters as well as in X^-H_2O (X = Br, I) clusters.[22−24] These characteristic lines have been assigned to "free OH groups interacting with the excess electron".[22−24] As shown by Figures 9 and 11, these lines, associated with the first solvation shell of the unpaired electron, are also prominent in H_3OW_n clusters. The existence of these fingerprint OH vibrations in H_3OW_{3m} clusters is a clear signature of the charge-separated structure of these species. Moreover, the value of ~2500 cm^{-1} found for the OH stretch vibration of the H_3O^+ unit in H_3OW_{3m} clusters is very close to that found for the OH stretch vibration of the hydronium cation in protonated water clusters.[31] This observation provides additional evidence of the charge-separation process in H_3OW_{3m} clusters.

To the knowledge of the authors, experimental IR spectra of size-selected H_3OW_n clusters have not yet been reported. Very

recently, the first transient mid-infrared spectra of the hydrated electron in water and heavy water have been obtained by Laenen et al.[74] A strong transient absorption positioned at ~2.9 μm (3450 cm^{-1}) in H_2O corresponds well in frequency and intensity to the present prediction for H_3OW_3 and H_3OW_6 clusters.

4. Conclusions

We have explored in this work the microsolvation of the hydronium radical using ab initio and DFT methods. The structures and the spectroscopic properties of selected H_3OW_n clusters have been discussed and compared with structures and spectra of the cluster cations. The conclusions of this investigation can be summarized as follows.

(i) Structures and vibrational spectra obtained with the DFT/B3LYP method are in good agreement with the results obtained with the ab initio MP2 method for the smaller clusters. This finding justifies the application of the cheaper DFT/B3LYP method for larger clusters.

(ii) The microsolvated hydronium cation can exist in both the Eigen-type structure, $H_3O^+W_n$, and the Zundel-type structure, $H_5O_2^+W_n$, depending on the local water environment. This is in accord with the results of previous computational studies.

(iii) The microsolvated hydronium radical prefers the Eigen-type structure, H_3OW_n, but the transition-state structure of the Zundel-type, $H_5O_2W_n$, is only marginally higher in energy in the case of closed solvation shells.

(iv) Microsolvation of the H_3O radical leads to a charge-separated complex, consisting of a hydronium cation and a localized electron cloud, which are connected by a water network. The particularly stable H_3O^+ species enforces a rather rigid structure of these complexes, especially for closed solvation shells, H_3OW_{3m}, $m = 1, 2, 3$. For the clusters investigated so far, the electron cloud localizes outside the water network, being solvated by a shell of water molecules.

(v) The H_3OW_3 cluster is considerably more stable than the bare H_3O radical with respect to the detachment of a hydrogen atom but is still a metastable species. The activation energy for the decomposition of the H_3OW_3 complex is estimated as 7 kcal/mol.

(vi) The vertical excitation energies of the s → p electronic transition of H_3OW_n clusters scatter between 1.1 and 3.0 eV. Complexation of H_3O with a single water molecule or three water molecules induces a large redshift of the s → p transition, which is followed by a gradual, but not monotonic, blue shift when additional water molecules are added. The sum of the oscillator strengths of the three s → p transitions is close to unity.

(vii) The microsolvated H_3OW_n clusters are predicted to exhibit a very intense (4000−6000 km/mol) OH stretch absorption in the range 3000−3500 cm^{-1}. This IR absorption represents the OH stretch vibration of the water molecules in the first solvation shell of the electron cloud.

Acknowledgment. This work has been supported by the Deutsche Forschungsgemeinschaft and the Committee for Scientific Research of Poland (Grant No. 3 T09A 082 19).

References and Notes

(1) Liu, K.; Brown, M. G.; Carter, C.; Saykally, R. J.; Gregory, J. K.; Clary, D. C. *Nature* **1966**, *381*, 501.
(2) Liu, K.; Cruzan, J. D.; Saykally, R. J. *Science* **1996**, *271*, 929.
(3) Buck, U.; Ettischer, I.; Melzer, M.; Buch, V.; Sadlej, J. *Phys. Rev. Lett.* **1998**, *80*, 2578.
(4) Brudermann, J.; Lohbrandt, P.; Buck, U.; Buch, V. *Phys. Rev. Lett.* **1998**, *80*, 2821.
(5) Liu, K.; Brown, M. G.; Saykally, R. *J. Phys. Chem. A* **1997**, *101*, 8995.
(6) Paul, J. B.; Provencal, R. A.; Chapo, C.; Roth, K.; Caseas, R.; Saykally, R. J. *J. Phys. Chem. A* **1999**, *103*, 2972.
(7) Keutsch, F. N.; Fellers, R. S.; Viant, M. R.; Saykally, R. J. *J. Chem. Phys.* **2001**, *114*, 3994.
(8) Gregory, J. K.; Clary, D. C. *J. Phys. Chem.* **1996**, *100*, 18014.
(9) Pedulla, J. M.; Kim, K.; Jordan, K. D. *Chem. Phys. Lett.* **1998**, *291*, 78.
(10) Schütz, M.; Rauhut, G.; Werner, H.-J. *J. Phys. Chem. A* **1998**, *102*, 5997.
(11) Jung, J. O.; Gerber, R. B. *J. Chem. Phys.* **1996**, *105*, 10332.
(12) Sadlej, J.; Buch, V.; Kazimirski, J. K.; Buck, U. *J. Phys. Chem. A* **1999**, *103*, 4933.
(13) Sadlej, J. *Chem. Phys. Lett.* **2001**, *333*, 485.
(14) Kryachko, E. S. *Chem. Phys. Lett.* **1999**, *314*, 353.
(15) Lee, H. M.; Suh, S. B.; Kim, K. S. *J. Chem. Phys.* **2001**, *114*, 10749.
(16) Smit, M. J.; Groenenboom, G. C.; Wormer, P. E. S.; van der Avoird, A.; Bukowski, R.; Szalewicz, K. *J. Phys. Chem. A* **2001**, *105*, 6212.
(17) Christiansen, O.; Nymand, T. M.; Mikkelsen, K. V. *J. Chem. Phys.* **2000**, *113*, 8101.
(18) Schwarz, H. A. *J. Chem. Phys.* **1977**, *67*, 5525.
(19) Yeh, L. I.; Okumura, M.; Myers, J. D.; Price, J. M.; Lee, Y. T. *J. Chem. Phys.* **1989**, *91*, 7319.
(20) Armbruster, M.; Haberland, H.; Schindler, H.-G. *Phys. Rev. Lett.* **1981**, *47*, 323.
(21) Coe, J. V.; Lee, G. H.; Eaton, J. G.; Arnold, S. T.; Sarkas, H. W.; Bowen, K. H.; Ludewigt, C.; Haberland, H.; Worsnop, D. R. *J. Chem. Phys.* **1990**, *92*, 3980.
(22) Ayotte, P.; Johnson, M. A. *J. Chem. Phys.* **1997**, *106*, 811.
(23) Bailey, C. G.; Kim, J.; Johnson, M. A. *J. Phys. Chem.* **1996**, *100*, 16782.
(24) Ayotte, P.; Weddle, G. H.; Bailey, C. G.; Johnson, M. A.; Vila, F.; Jordan, K. D. *J. Chem. Phys.* **1999**, *110*, 6268.
(25) Maeyama, T.; Tsumura, T.; Fujii, A.; Mikami, N. *Chem. Phys. Lett.* **1997**, *264*, 292.
(26) Atkins, P. *Physical Chemistry*, 6th ed.; Oxford University Press: Oxford, U.K., 1998; Section 24.8.
(27) Eigen, M. *Angew. Chem., Int. Ed. Engl.* **1964**, *3*, 1.
(28) Zundel, G. In *The Hydrogen Bond - Recent Developments in Theory and Experiments*. *II. Structure and Spectroscopy*; Schuster, P., Zundel, G., Sandorf, C., Eds.; North-Holland: Amsterdam, 1976; pp 683−766.
(29) Tomoda, S.; Kimura, K. *Chem. Phys.* **1983**, *82*, 215.
(30) Xie, Y.; Remington, R. B.; Schaefer, H. F., III *J. Chem. Phys.* **1994**, *101*, 4878.
(31) Wei, D.; Salahub, D. R. *J. Chem. Phys.* **1994**, *101*, 7633.
(32) Muguet, F. F. *J. Mol. Struct.* (*THEOCHEM*) **1996**, *368*, 173.
(33) Geissler, P.; Voorhis, T. V.; Dellago, C. *Chem. Phys. Lett.* **200**, *324*, 149.
(34) Ciobanu, C. V.; Ojmae, L.; Shavitt, I.; Singer, S. J. *J. Chem. Phys.* **2000**, *113*, 5321.
(35) Tuckerman, M. E.; Marx, D.; Klein, M. L.; Parinello, M. *Science* **1997**, *275*, 817.
(36) Marx, D.; Tuckerman, M. E.; Hutter, J.; Parinello, M. *Nature* **1999**, *397*, 601.
(37) Kobayashi, C.; Saito, S.; Ohmine, I. *J. Chem. Phys.* **2000**, *113*, 9090.
(38) Walbran, S.; Kornyshev, A. A. *J. Chem. Phys.* **2001**, *114*, 10039.
(39) Hart, E. J.; Anbar, M. *The Hydrated Electron*; Wiley: New York, 1970.
(40) Fang, D. F.; Kevan, L. *Chem. Rev.* **1980**, *80*, 1.
(41) Smith, D. M. A.; Smets, J.; Elkadi, Y.; Adamowicz, L. *J. Chem. Phys.* **1997**, *107*, 5788; **1998**, *109*, 1238; **1999**, *110*, 3804.
(42) Lee, S.; Kim, J.; Lee, S. J.; Kim, K. S. *Phys. Rev. Lett.* **1997**, *79*, 2038.
(43) Tsurusawa, T.; Iwata, S. *Chem. Phys. Lett.* **1998**, *287*, 553.
(44) Weigend, F.; Ahlrichs, R. *Phys. Chem. Chem. Phys.* **1999**, *1*, 4537.
(45) Kulkarni, S. A.; Bartolotti, L. J.; Pathak, R. K. *J. Chem. Phys.* **2000**, *113*, 2697.
(46) Niblaeus, K. S. E.; Roos, B. O.; Siegbahn, P. E. M. *Chem. Phys.* **1977**, *25*, 207.
(47) Talbi, D.; Saxon, R. P. *J. Chem. Phys.* **1989**, *91*, 2376.
(48) Gellene, G. I.; Porter, R. F. *J. Chem. Phys.* **1984**, *81*, 5570.
(49) Hudgins, D. M.; Porter, R. F. *Int. J. Mass Spectrom. Ion Processes* **1994**, *130*, 49.
(50) McLoughlin, P. W.; Gellene, G. I. *J. Phys. Chem.* **1992**, *96*, 4396.
(51) Luo, M.; Jungen, M. *Chem. Phys.* **1999**, *241*, 297.
(52) Herzberg, G. *Faraday Discuss. Chem. Soc.* **1981**, *71*, 165.
(53) Schwartz, M. E. *Chem. Phys. Lett.* **1976**, *40*, 1.
(54) Muguet, F. F.; Gelabert, H.; Gauduel, Y. *J. Chim. Phys.* **1996**, *93*, 1808.
(55) http://www.ensta.fr/~muguet.

(56) Alagia, M.; Balucani, N.; Casavecchia, P.; Stranges, D.; Volpi, G. G.; Clary, D. C.; Kliesch, A.; Werner, H. J. *Chem. Phys*. **1996**, *207*, 389.

(57) Wu, G. S.; Schatz, S. C.; Lendvay, G.; Fang, D. C.; Harding, L. B. *J. Chem. Phys*. **2000**, *113*, 3150.

(58) Bettens, R. P. A.; Collins, M. A.; Jordan, M. J. T.; Zhang, D. H. *J. Chem. Phys*. **2000**, *112*, 10162.

(59) Lester, M. I.; Loomis, R. A.; Schwartz, R. L.; Walch, S. P. *J. Phys. Chem. A* **1997**, *101*, 9195.

(60) Dedonder-Lardeux, C.; Grosswasser, D.; Jouvet, C.; Martrenchard, S. *Phys. Chem. Chem. Phys.* **2001**, *4*, 1.

(61) Pino, G.; Gregoire, G.; Dedonder-Lardeux, C.; Jouvet, C.; Martrenchard, S.; Solgadi, D. *Phys. Chem. Chem. Phys.* **2000**, *2*, 893.

(62) Gregoire, G.; Dedonder-Lardeux, C.; Jouvet, C.; Martrenchard, S.; Solgadi, D. *J. Phys. Chem. A* **2001**, *105*, 5971.

(63) Ishiuchi, S.; Saeki, M.; Sakai, M.; Fujii, M. *Chem. Phys. Lett*. **2000**, *322*, 27.

(64) Sobolewski, A. L.; Domcke, W. *Chem. Phys. Lett*. **2000**, *321*, 479.

(65) Sobolewski, A. L.; Domcke, W. *Chem. Phys. Lett*. **2000**, *329*, 130.

(66) Sobolewski, A. L.; Domcke, W. *J. Phys. Chem. A* **2001**, *105*, 9275.

(67) Grossweiner, L. I.; Swenson, G. W.; Zwicker, E. F. *Science* **1963**, *141*, 805.

(68) Bent, D. V.; Hayon, E. *J. Am. Chem. Soc.* **1975**, *97*, 2599.

(69) Muguet, F.; Bassez, M.-P.; Robinson, G. W. *J. Phys. Chem.* **1988**, *92*, 7262.

(70) Sobolewski, A. L.; Domcke, W. *Phys. Chem. Chem. Phys*. **2002**, *4*, 4.

(71) Frisch, M. J.; Trucks, G. W.; Schlegel, H. B.; Scuseria, G. E.; Robb, M. A.; Cheeseman, J. R.; Zakrzewski, V. G.; Montgomery, J. A., Jr.; Stratmann, R. E.; Burant, J. C.; Dapprich, S.; Millam, J. M.; Daniels, A. D.; Kudin, K. N.; Strain, M. C.; Farkas, O.; Tomasi, J.; Barone, V.; Cossi, M.; Cammi, R.; Mennucci, B.; Pomelli, C.; Adamo, C.; Clifford, S.; Ochterski, J.; Petersson, G. A.; Ayala, P. Y.; Cui, Q.; Morokuma, K.; Malick, D. K.; Rabuck, A. D.; Raghavachari, K.; Foresman, J. B.; Cioslowski, J.; Ortiz, J. V.; Stefanov, B. B.; Liu, G.; Liashenko, A.; Piskorz, P.; Komaromi, I.; Gomperts, R.; Martin, R. L.; Fox, D. J.; Keith, T.; Al-Laham, M. A.; Peng, C. Y.; Nanayakkara, A.; Gonzalez, C.; Challacombe, M.; Gill, P. M. W.; Johnson, B. G.; Chen, W.; Wong, M. W.; Andres, J. L.; Head-Gordon, M.; Replogle, E. S.; Pople, J. A. *Gaussian 98*; Gaussian, Inc.: Pittsburgh, PA, 1998.

(72) Andersson, K.; Roos, B. O. In *Modern Electronic Structure Theory*; Yarkony, D. R., Ed.; World Scientific: Singapore, 1995; p 55.

(73) Andersson, K. et al. *MOLCAS User's Guide*, version 4; University of Lund: Lund, Sweden, 1997.

(74) Laenen, R.; Roth, T.; Lauberau, A. *Phys. Rev. Lett*. **2000**, *85*, 50.